3-2019

Latent Sensitization in a Mouse Model of Ocular Neuropathic Pain

Jooyoung Cho
University of Kentucky, jooyoung.cho@uky.edu

Nicholas Bell
University of Kentucky

Gregory Botzet
University of Kentucky, gjbotz2@uky.edu

Paras Vora
University of Kentucky, paras.vora@uky.edu

Benjamin J. Fowler
University of Miami

See next page for additional authors

Right click to open a feedback form in a new tab to let us know how this document benefits you.

Follow this and additional works at: https://uknowledge.uky.edu/ophthalmology_facpub

Part of the Analytical, Diagnostic and Therapeutic Techniques and Equipment Commons, and the Ophthalmology Commons

Authors

Jooyoung Cho, Nicholas Bell, Gregory Botzet, Paras Vora, Benjamin J. Fowler, Renee R. Donahue, Heather M. Bush, Bradley K. Taylor, and Romulo J. C. Albuquerque

Latent Sensitization in a Mouse Model of Ocular Neuropathic Pain

Article

Latent Sensitization in a Mouse Model of Ocular Neuropathic Pain

Jooyoung Cho[1], Nicholas Bell[1], Gregory Botzet[1], Paras Vora[1], Benjamin J. Fowler[2], Renee Donahue[3], Heather Bush[4], Bradley K. Taylor[3,5], and Romulo J. C. Albuquerque[1]

[1] Department of Ophthalmology, University of Kentucky, Lexington, KY, USA
[2] Bascom Palmer Eye Institute, University of Miami Miller, Miami, FL, USA
[3] Department of Physiology, University of Kentucky, Lexington, KY, USA
[4] Department of Biostatistics, University of Kentucky, Lexington, KY, USA
[5] Department of Anesthesiology, University of Pittsburgh, PA, USA

Purpose: Chronic ocular pain is poorly understood and difficult to manage. We developed a murine model of corneal surface injury (CSI)–induced chronic ocular neuropathic pain. The study focuses on changes in corneal nerve morphology and associated short- and long-term pain-like behavior after CSI.

Methods: CSI was induced in mice by local application of an alkali solution (0.75 N NaOH). Corneal nerve architecture, morphology, density, and length were studied. Eye-wiping was evaluated before and after CSI in response to hypertonic saline (2 M NaCl). Naltrexone (NTX) or Naloxone-methiodide (NLX-me), opioid receptor antagonists, were given subcutaneously (s.c., 3 mg/kg) or topically (eye drop, 100 μM), and then an eye-wiping test was performed.

Results: CSI caused partial corneal deinnervation followed by gradual reinnervation. Regenerated nerves displayed increased tortuosity, beading, and branching. CSI enhanced hypertonic saline-induced eye-wiping behavior compared to baseline or sham-injury ($P < 0.01$). This hypersensitivity peaked at 10 days and subsided 14 days after CSI. Administration of NTX, or NLX-me, a selective peripheral opioid antagonist, reinstated eye-wiping behavior in the injury group, but not in the sham groups ($P < 0.05$).

Conclusions: This study introduces a model of chronic ocular pain and corneal neuropathy following CSI. CSI induces central and peripheral opioid receptor-dependent latent sensitization (LS) that is unmasked by systemic or topical administration of opioid antagonists.

Translational Relevance: This model of chronic ocular pain establishes LS as a new inhibitory mechanism in the oculotrigeminal system and may be used for potential diagnostic and therapeutic interventions for ocular neuropathy.

Introduction

Ocular neuropathic pain is a poorly treatable, debilitating condition that negatively impacts the quality of life of millions in the United States.[1,2] Numerous, diverse etiologies exist for ocular neuropathic pain that are broadly classified by nature of insult (mechanical, thermal, chemical, or infectious), and usually involve pathology of the cornea, a densely innervated tissue.[3,4] Emerging evidence indicates that corneal sensory neuropathy is a common underlying mechanism of ocular neuropathic pain.[5–7] However, despite an increasing recognition of the importance and prevalence of ocular neuropathic pain, diagnosis and management remain challenging due to a paucity of clinical correlates on ophthalmologic exam, as well as the need to better understand underlying neurobiology and pathophysiology.

A major limitation to existing ocular pain models (e.g., humidity chambers, topical pollutant or BAC

administration, corneal cauterization, oral finasteride, or extraorbital lacrimal gland excision) is that they assess predominantly acute pain behaviors that are short-lived.[8–13] Given that ocular neuropathic pain follows a chronic and relapsing–remitting course,[14] we developed an animal model that better recapitulates the chronicity of ocular neuropathic pain.

Nociceptive signals in chronic neuropathy are mediated by inflammation and/or tissue damage that enhances the sensitivity of peripheral neurons (peripheral sensitization) and central neurons.[15] Nerve injury causes chronic neuronal sensitization via long-term potentiation of nociceptive neurons. Recent studies have established that chronic nerve sensitization is silenced by endogenous opioid receptors in a process known as latent pain sensitization (LS). Opioid receptor antagonism disrupts LS and reinstates pain precipitating cellular, somatic, and aversive signs of physical withdrawal in animals. Therefore, LS is an important pain inhibitory mechanism, but also represents a state of increased susceptibility to pain reinstatement.[16,17] Whether this adaptive response contributes to chronic ocular pain after injury to the corneal surface has not been established to our knowledge.

We established a model of sustained ocular hypersensitivity associated with corneal neuropathic changes. It combines local application of an alkali solution to induce a controlled corneal surface injury (CSI) with topical application of a hypertonic saline solution to elicit eye-wiping behavior. We also defined the anatomic pathology in corneal nerve fiber layers in terms of nerve density, length, and architecture throughout 42 days after injury. Finally, the opioid receptor inverse agonists, naltrexone (NTX) and naloxone-methiodide (NLX-me), are used to test whether LS contributes to chronic ocular pain.

Methods

Animals

Male C57BL/6 mice were purchased from the Jackson Laboratory (Bar Harbor, ME) and studied beginning at 8 weeks of age. All animal-based procedures were performed in accordance with the Association of Research in Vision and Ophthalmology (ARVO) Statement for the Use of Animals in Ophthalmic and Vision Research and the National Institute of Health (NIH; Bethesda, MD) *Guide for the Care and use of Laboratory Animals*. The experimental

protocol was approved by the institutional animal care committee for animal research of the University of Kentucky.

Corneal Surface Injury (CSI)

All mice were anesthetized with an intraperitoneal (i.p.) injection of ketamine (125 mg/kg)/ xylazine (7 mg/kg). Deep anesthesia was confirmed by lack of response to toe pinch. Alkali-immersed filter discs were used to induce corneal injury in mice.[18] Whatman filter paper was used to prepare discs with 4 mm diameter. Filter paper discs were soaked in sodium hydroxide solution (NaOH; pH 13.0 ± 0.05; 0.25 N, 0.75 N, 1 N) for 10 seconds. The discs then were blotted with a paper towel to remove excess NaOH solution. The wet filter paper discs were placed on the center of the corneal surface for 10 seconds. The contact area between the disc and cornea was limited to a central circle of approximately 2 mm diameter. After its removal, the entire ocular surface was irrigated immediately with 10 mL balanced salt solution (BSS), using a 10 mL syringe with an 18-gauge (G) blunt needle. The corneal surface then was massaged gently with the smooth side of forceps to remove damaged tissue. Afterwards, a second round of irrigation to the entire ocular surface was performed with an additional 10 mL BSS. After debridement, neomycin and polymyxin B sulfate (Bausch & Lomb, Inc., Tampa, FL) were applied to the entire ocular surface of both eyes to prevent dryness and infection. For the sham group, neomycin and polymyxin B sulfates were applied after anesthesia was induced. After these procedures, mice were placed on a heating pad until fully awake and then returned to their home cage.

Behavioral Study

Testing Apparatus

Two frameless square mirrors were linked together at a 60° angle by a metal hinge. A clear open-top acrylic cylinder with a 13.5 cm diameter and 17 cm height was placed between the mirrors. The mouse was placed inside the clear cylinder and its reflection was shown on the mirrors, which allowed visualization of the face regardless of the mouse position. The bottom of the cylinder was covered with a circular filter paper, which was replaced before each subsequent testing. A video camera was placed in front of the cylinder and behavioral responses were recorded (Supplementary Fig. S1).

Eye-wiping Test

One week before measuring the baseline, mice were habituated to the testing environment for 10 minutes on three separate days. On testing days, mice were first acclimated to the testing apparatus for 10 minutes. Then, mice were grasped gently and one drop of sodium chloride solution (NaCl; pH 7.4 ± 0.05; 1, 2, or 3 M) was applied to the center of the corneal surface of the right eye, using a 25 G needle attached to a BSS bottle; care was taken to avoid touching the ocular surface. Ten seconds after application of NaCl, mice were returned to the testing apparatus and the number of eye wipes performed with the ipsilateral forepaw was counted for 30 seconds duration. Hind paw wipes/scratches were very rare and not included. Next, the entire ocular surface was irrigated with 10 mL BSS, and mice were returned to their home cage.

Drug Administration

NTX hydrochloride (cat. No. 0677; TOCRIS, Bristol, United Kingdom) was subcutaneously (s.c.) administered (3 mg/kg in BSS) in a volume of 10 mL/kg and eye-wipe testing was performed with 2 M NaCl at 30 minutes after administration of NTX. NTX dosing and timing were performed as previously reported by Corder et al.[17] NLX-me (cat. No. N129; Sigma-Aldrich Corp., St. Louis, MO) was topically instilled (100 μM in BSS) and eye-wiping test was performed 50 minutes after instillation of NLX-me eye drop. Dosing of NLX-me was based on previous published work on the topical application NTX at 100 μM dose.[19] Hypersensitivity after NLX-me was not observed until 50 minutes after instillation.

Immunofluorescence Staining and Imaging of the Whole Cornea Flat Mount

Animals ($n = 3$ for each time point) were euthanized. Then, the eyes were enucleated and fixed in freshly prepared 4% paraformaldehyde (PFA) for 15 minutes. The corneas were excised along the limbus and fixed in 4% PFA for 45 minutes, followed by two washes in $1 \times$ PBS for 5 minutes per wash. The corneas then were placed in ice-cold methanol for 20 minutes, followed by two washes with $1 \times$ PBS for 10 minutes per wash. To block nonspecific binding, corneas were incubated with blocking solution (10% normal goat serum, 3% bovine serum albumin [BSA], 1% Triton-X, 0.05% Tween 20, 0.05% sodium azide) in $1 \times$ PBS overnight at 4°C. The corneas then were incubated with rabbit anti-β III-tubulin antibody (18207; 1:200; Abcam, Cambridge, UK) for 72 hours at 4°C, followed by incubation with goat anti-rabbit Alexa Fluor 488 (1:200; (EMD Millipore, Burlington, MA) for 2 hours at room temperature. After washing with $1 \times$ PBS three times (10 minutes/wash), four radial cuts were made to the whole cornea to flatly mount it on a slide with the endothelium side down, and then cover slipped with ProLong Gold antifade reagent without 4′,6-diamidino-2-phenylendole (DAPI).

Three-dimensional (3D) reconstruction of the corneal nerve networks was performed with confocal microscopy (1 μm slices). The central 2×2 mm square was imaged from the epithelial to the stromal layer (Nikon Eclipse A1R+; Nikon Corp., Tokyo, Japan) with a ×20 and ×60 objective lens. The images obtained from the same layer of the cornea were merged.

Nerve fiber density and length were assessed in the central 4 mm^2 area in the epithelial, subbasal, and stromal layers of each cornea. Density was calculated using ImageJ software as previously described[20] and length was calculated using Angio Tool software.[21] This was performed in sham- and alkali-treated corneas at 2, 10, 21 and 42 days after injury.

pERK Stimulation and Staining

To identify sensitized neurons in the trigeminal ganglion (TG), 2 M NaCl solution was instilled onto the mouse right eye in all groups except a naïve group. Anesthesia and perfusion were completed within 10 minutes post 2M NaCl application.

Mice deeply anesthetized with ketamine (125 mg/kg)/xylazine (7 mg/kg) were perfused with ice-cold BSS, and then fixed by ice-cold 4% PFA. Following perfusion and fixation, the head was decapitated and the TG tissue was harvested. The TG tissue was postfixed in 4% PFA for 1 hour. After serial washes in $1 \times$ PBS, TG tissue was cryoprotected in 15% sucrose overnight. Next day, TG was embedded in Tissue-Tek optimal cutting temperature (OCT) compound and stored at −80°C. Frozen TG tissue then was sectioned into 10 μM thickness at −30°C, using the cryostat.

The TG then was sectioned in 10 μm slices from its dorsal surface and the 15th section located approximately 150 μm deep. This slice, which contains the greatest number of neuronal cell bodies from corneal afferents, was used for neuronal activation quantification.[22] TG sections were treated with blocking solution (2% normal donkey serum, 1% BSA, 0.1% Triton-X, 0.05% Tween 20, 0.05% sodium azide in BSS) for 1 hour at room temperature, followed by overnight incubation with Alexa Fluor 488-conjugated mouse anti-NeuN (MAB377X; EMD Millipore)

and rabbit anti-pERK (4370; Cell Signaling Technology, Danvers, MA) antibodies at 4°C. Next day, sections were washed in $1 \times$ PBS twice and incubated in donkey anti-rabbit secondary antibody conjugated with Alexa Fluor 594 for 2 hours at room temperature. After serial washes in $1 \times$ PBS, sections were cover-slipped with anti-fade ProLong Gold containing DAPI. Images were captured using the confocal microscope (Nikon Eclipse A1R+; Nikon Corp.) with a ×20 objective lens.

Data Analysis

Behavioral Study Data

One-way ANOVA was used to compare the area under the curve (AUC) of multiple NaOH doses within the same concentration of NaCl, and then post hoc Tukey tests were performed. Linear mixed models were used to compare group means while accounting for correlation that occurs with repeated measurement using SAS v9.4. Covariance structure was selected using information criteria where smaller is better. Results are presented as the mean ± standard error of the mean (SEM); for repeated measures analysis with significant time-group interactions group means are presented by time point. $P \leq 0.05$ was considered a statistically significant difference among groups.

Nerve Fiber Quantification Data

An analysis was performed at each layer (epithelial, subbasal, and stromal). One-way ANOVA was used to compare the density of corneal nerve fibers in injury group at multiple time points and post hoc Tukey tests then were performed. Student's t-test compared the length of corneal nerve fibers in sham and injury groups. Results are presented as the mean ± SEM. $P \leq 0.05$ was considered a statistically significant difference among groups.

pERK Quantification Data.

Two blinded examiners independently counted the total number of NeuN-positive neurons as well as of pERK-positive cells that are colocalized with NeuN within V1 area in each TG. Then, the number of pERK-positive neurons was divided by the number of NeuN-positive neurons, multiplied by 100 to find % pERK positive neurons.

$$\% \text{ pERK positive neurons} = \frac{\text{number of pERK positive neurons}}{\text{number of NeuN positive neurons}} \times 100$$

Student's t-test was used to compare the mean %pERK-positive neurons between the two groups.

# Results

CSI Causes Ocular Hyperalgesia

The alkali burn model of CSI was used to study corneal sensitivity.[18] In this model, mice underwent an alkali burn injury with a NaOH-soaked filter paper disc and eyes were tested for hypersensitivity with measurement of eye-wiping behavior following corneal application of a drop of NaCl hypertonic saline.[23] To identify the optimal concentration of injury and stimulus, we tested multiple concentrations of NaOH and NaCl solutions: vehicle or NaOH (0.25, 0.75, and 1.0 N) and NaCl (1, 2, and 3M). Preliminary testing of the highest NaOH concentration (1 N) caused corneal perforation in four of six mice tested and, therefore, was excluded.

Eye-wiping behavior was assessed at baseline, and 2, 4, 7, 10, 14, and 21 days after CSI, and the AUC from the baseline to day 21 was calculated (Fig. 1A). Interestingly, when 1 M NaCl or 3 M NaCl solution was used as stimulus, sham and CSI groups (0.25 N NaOH, 0.75 N NaOH) showed similar eye-wiping behavior (Fig. 1A). We concluded that 1 M NaCl may not be noxious enough to generate robust response in the CSI group. In contrast, 3 M NaCl solution could be too strong and elicited high wiping behavior in sham and CSI groups. We found, however, that 2 M NaCl stimulation resulted in a robust increase in 0.75 N NaOH-treated CSI animals compared to sham controls (Fig. 1A, overall $P < 0.01$; sham vs. 0.75 N NaOH; $P < 0.05$). Thus, all subsequent experiments were performed using this combination of injury and stimulus intensities.

We next evaluated the time course of CSI-induced ocular hyperalgesia. Overall, the groups changed differently over time (Fig. 1B, group*time, $P < 0.05$). Specifically, the CSI group significantly increased the number of eye wipes at post-injury day 10 compared to the baseline level (Fig. 1B, $P < 0.01$) and the sham group (Fig. 1B, $P < 0.05$). At day 21, hyperalgesic behavior in the CSI group returned to baseline for up to 42 days after injury, consistent with remission of ocular hyperalgesia (Fig. 1B). In contrast, no changes in eye-wiping were noted in the sham group throughout the 42 days (Fig. 1B, $P > 0.05$).

CSI-Induced Corneal Neuropathy

To determine the degree and duration of corneal nerve disturbance after CSI, we evaluated the architecture of corneal nerves at different time points
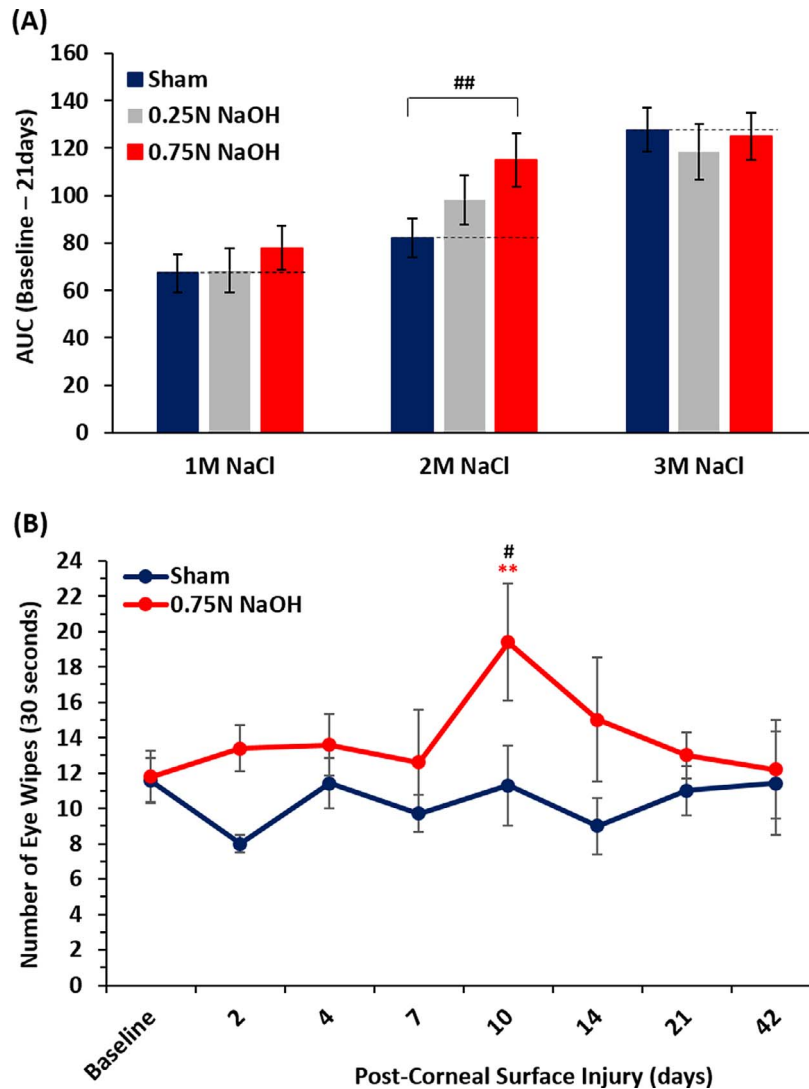
Figure 1. Corneal surface injury causes ocular hyperalgesia. (A) AUC for eye-wiping behavior from baseline through 2, 4, 7, 10, 14 days to 21 days after CSI in sham and CSI groups (0.25 N NaOH, 0.75 N NaOH) with three different concentrations of NaCl solutions (1, 2, and 3M). One-way ANOVA was used to compare AUC of NaOH doses within the same concentration of NaCl, and then post hoc Tukey tests were performed (##$P< 0.01$). (B) Number of eye wipes in sham ($n = 7$) and CSI (0.75 N NaOH; $n = 5$) groups at baseline and 2, 4, 7, 10, 14, 21, and 42 days after CSI after an application of 2 M NaCl. Linear mixed models were used to compare the groups over time (between sham and CSI: #$P < 0.05$, within CSI: **$P < 0.01$). The data are presented as mean±SEM.

by calculating corneal nerve density in epithelial, subbasal, and stromal layers independently ($n = 3$ corneas/time point; Figs. 2–4). Representative images of the entire cornea are shown on Supplementary Figure S2. Two days after CSI, corneal nerve density was significantly decreased in all three layers of the cornea compared to baseline (Figs. 2–4, $P < 0.01$). In particular, this effect was most dramatic in the epithelial layer of the cornea where nerve-like structures were not observed. On subsequent time-points, the density of nerves gradually increased in a time-dependent manner. By 42 days after CSI, the

epithelial and stromal layers were fully reinnervated compared to baseline; however, density in the subbasal region remained relatively low compared to sham (Figs. 2–4, $P < 0.01$).

Although the central cornea remained relatively denervated at 42 days after CSI (red circle; Fig. 5B), the epithelial nerve density returned to baseline (Fig. 2A). Therefore, we sought to evaluate the morphology of corneal nerves in each layer separately. The distribution and arrangement of nerve terminals were dramatically altered with increased length (Fig. 5C) and presence of neuroma-like structures (Figs. 5IIIa,
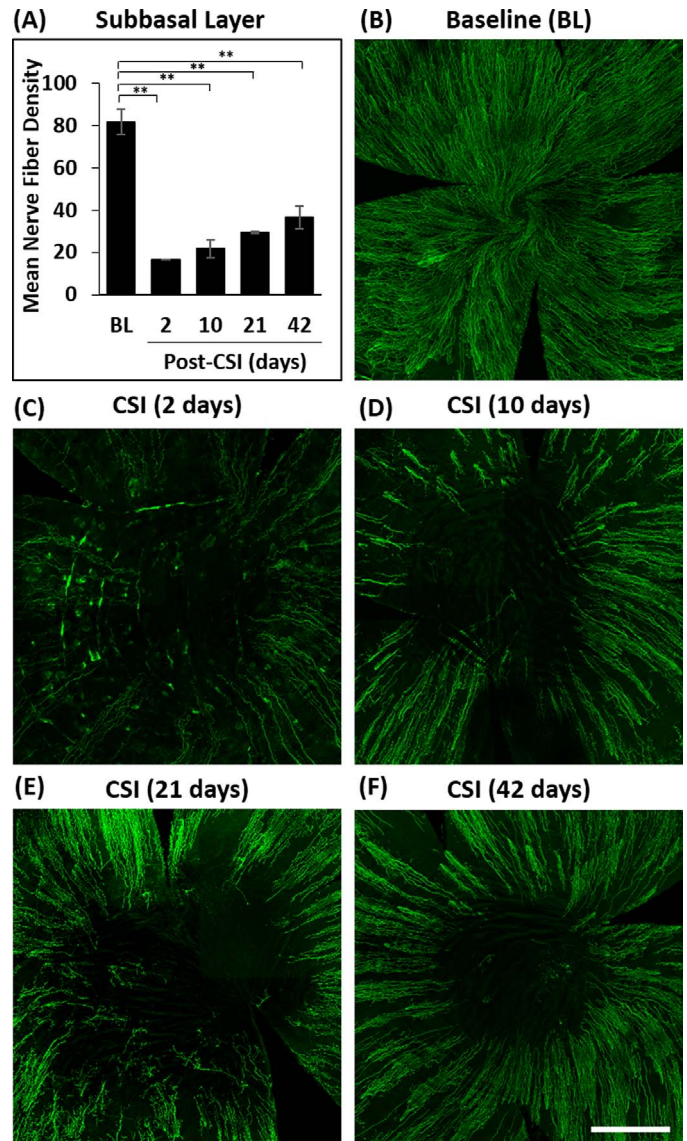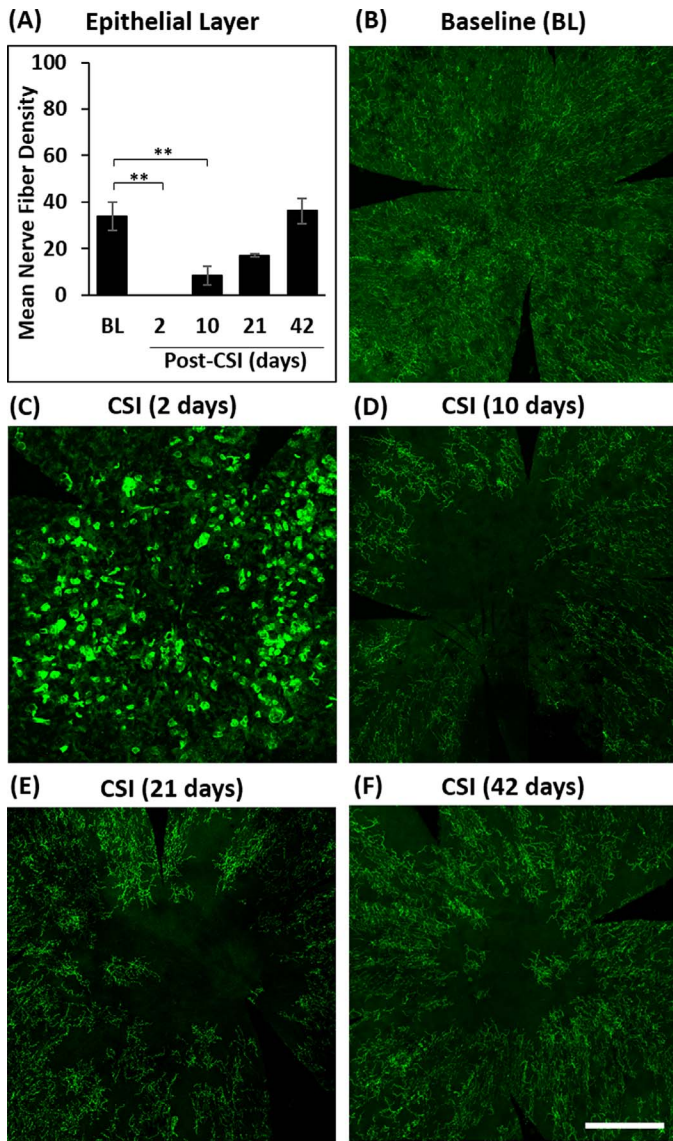
Figure 2. Evaluation of corneal nerves in the epithelial layer following corneal surface injury. (A) Density of mouse corneal nerve endings in the epithelial layer at baseline, 2, 10, 21 and 42 days after CSI ($n = 3$ for each time point). One-way ANOVA was used to compare the density of corneal nerve fibers and post hoc Tukey tests then were performed. (**$P < 0.01$). The data are presented as mean±SEM. (B–F) Representative images of epithelial layer on cornea whole mounts (2×2 mm^2) with free nerve endings labeled with anti-beta III tubulin (*green*). *Scale bar*: 500 μm.

Figure 3. Examination of corneal nerves in the subbasal layer following corneal surface injury. (A) Density of mouse corneal nerve fibers in the subbasal layer at baseline, and 2, 10, 21, and 42 days after CSI ($n = 3$ for each time point). One-way ANOVA was used to compare the density of corneal nerve fibers and post hoc Tukey tests then were performed (**$P < 0.01$). The data are presented as mean±SEM. (B–F) Representative images of subbasal layer of cornea whole mounts (2×2 mm^2) with nerve plexus labeled with anti-beta III tubulin (*green*). *Scale bar*: 500 μm.

5IVa). Nerves in the peripheral subbasal and stromal layers showed increased beading (arrow) and tortuosity (Figs. 5Ib–IVb, 5Ic–IVc). The 3D reconstruction images (Figs. 5Id–IVd) revealed that neuroma-like structures in the epithelial layer of the injured corneas were originating directly from stromal nerves bypassing the diminished subbasal plexus. In regard to nerve length, while the epithelial terminals became longer

after injury, the subbasal layer had shorter nerve fibers and the stromal layer was unchanged (Fig. 5C). Together, these data indicated that CSI caused a rearrangement in corneal nerves resulting in structural abnormalities including neuroma formation in the epithelial layer, profound loss of nerve density in the subbasal nerves and increasing beading and tortuosity of stromal nerve trunks.
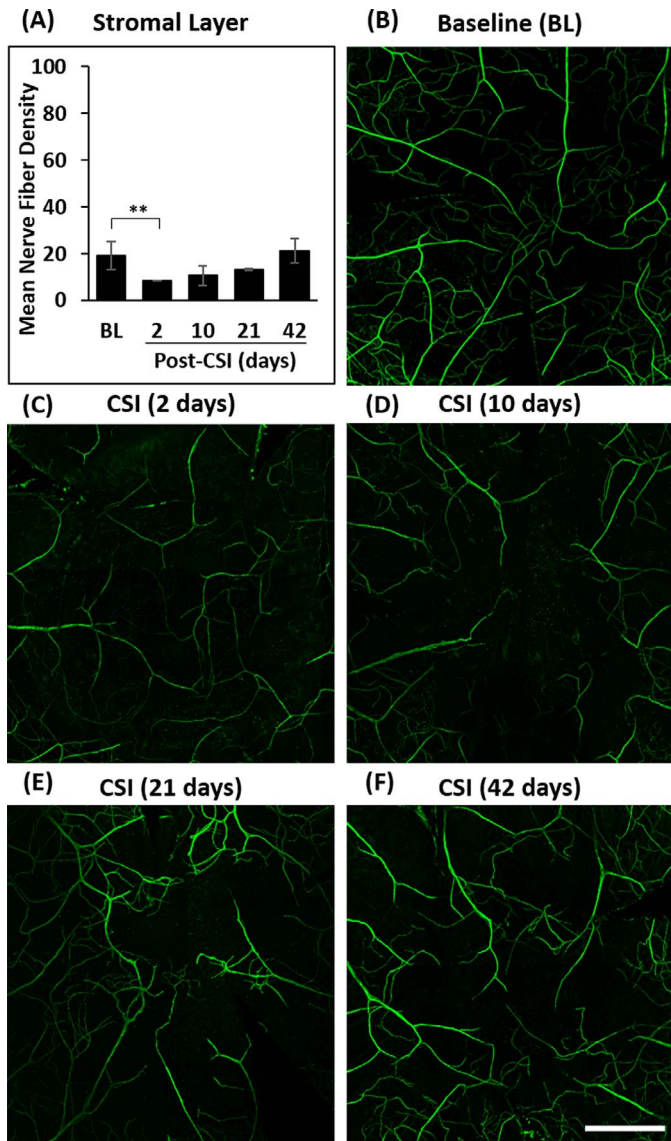
Figure 4. Assessment of the corneal stromal nerves following corneal surface injury. (A) Density of mouse corneal nerve fibers in the stromal layer at baseline, and 2, 10, 21, and 42 days after CSI ($n = 3$ for each time point). One-way ANOVA was used to compare the density of corneal nerve fibers and post hoc Tukey tests then were performed (**$P < 0.01$). The data are presented as mean±SEM. (B-F) Representative images of nerve trunks in central 2×2 mm^2 area of the stromal layer on corneal whole mounts stained with anti-beta -III tubulin (*green*). *Scale bar*: 500 μm.
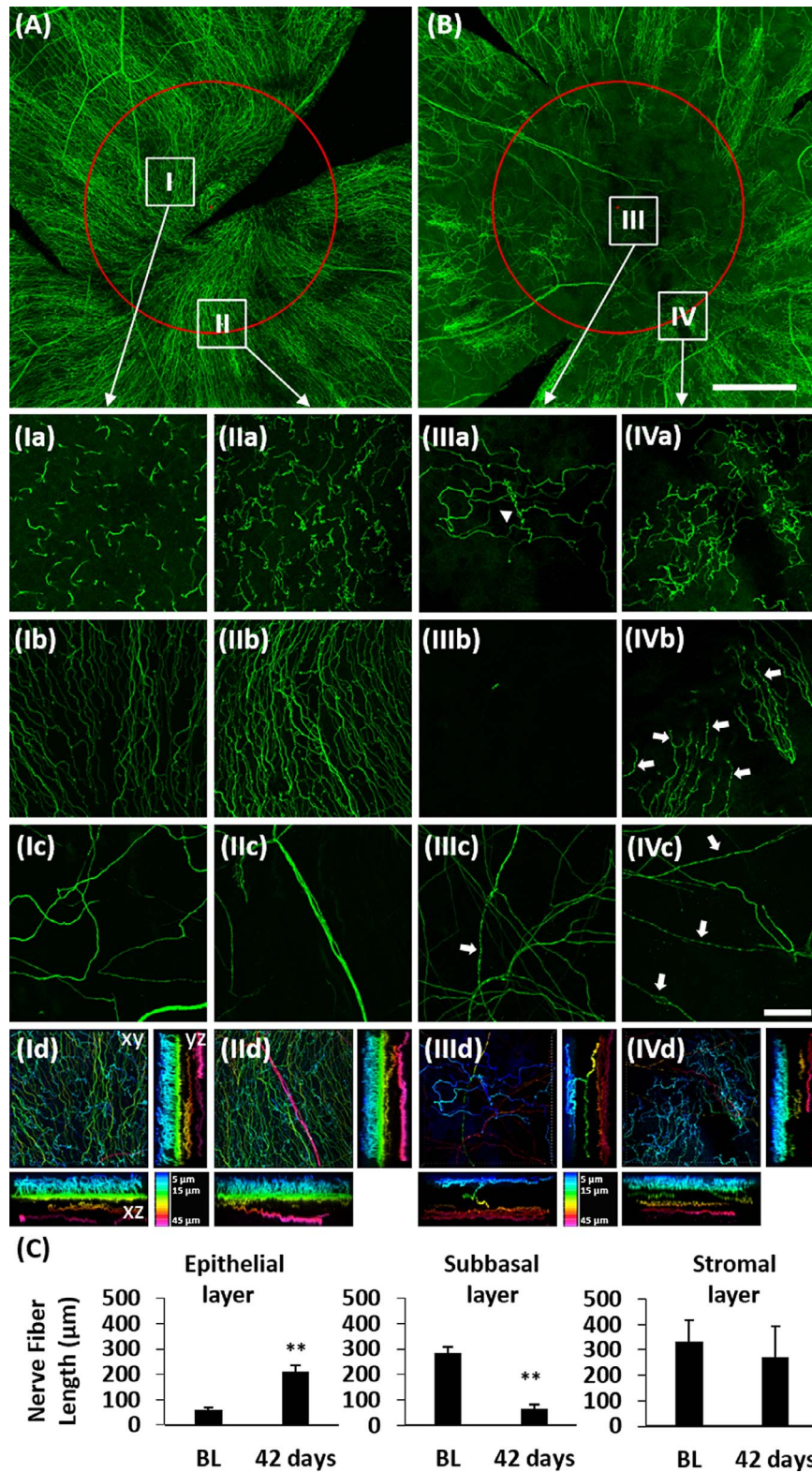
CSI Induces Peripheral LS

We were intrigued that despite numerous maladaptive changes in the corneal nerve architecture after corneal injury (i.e., increased tortuosity, beading, and loss of subbasal nerve density shown in Figs. 2–5), pain behavior subsided within 14 days of injury

and did not spontaneously reinstate for up to 6 weeks after injury (Fig. 1B). We hypothesized that endogenous opioid receptor signaling contributes to this remission of nociceptive behavior, as described in models of LS.[17,24] To test this hypothesis, we administered the global opioid antagonist/inverse agonist, NTX, at 7 weeks after CSI when the pain behavior resolved. As illustrated in Figure 6A, naltrexone reinstated peak eye-wipe behavior in the CSI group, but not in the sham group ($P < 0.05$). Although LS is well established in the spinal cord and brain, we asked the question whether, in our model, NTX-induced reinstatement was paralleled by peripheral sensitization at the TG.[17,25] We showed that systemic NTX administration caused increased immunoreactivity to pERK, a marker of neuronal activation, within NeuN-positive cells (neurons) at the ophthalmic division of the TG in CSI mice compared to sham mice (Figs. 6B, 6C, Supplementary Fig. S3) or naive animals (Supplementary Fig. S4).

To further test whether LS could be partly mediated by the peripheral LS, we studied the effect of NLX-me, an opioid antagonist that does not cross the blood–brain barrier. One drop of NLX-me (100 μM) applied to the ocular surface at 16 weeks after CSI reinstated the ocular pain behavior in the CSI mice, but had no effect in uninjured mice (Fig. 7). These results suggest that peripheral endogenous opioid receptor activation masks a sustained but silent ocular hyperalgesia induced by CSI.

Discussion

Alkali burn to the ocular surface has been widely used to study corneal neovascularization, wound healing, and inflammation.[18,26–28] Tissue injury and remodeling beyond the ocular surface including retinal and optic nerve gliosis also have been reported after alkali injury to the cornea.[26,28–31] Although alkali burn causes corneal nerve damage and significant pain in patients, little is known about the long-term effects of alkali burn injury to the oculotrigeminal sensory system.[32] In this study, we repurposed this injury model to study ocular sensitivity by combining CSI with application of NaCl to the cornea. The application of hypertonic saline to the ocular surface elicited an eye-wiping response that reflects an ongoing stimulation of nociceptors in the cornea.[23,33] Beyond studying short-term changes in corneal nerves and ocular sensitivity, we determined the long-term effects of CSI by establishing how LS develops after ocular injury.

(A)

I

II

(B)

III

IV

(Ia) **(IIa)** **(IIIa)** **(IVa)**

(Ib) **(IIb)** **(IIIb)** **(IVb)**

(Ic) **(IIc)** **(IIIc)** **(IVc)**

(Id) xy yz **(IId)** **(IIId)** **(IVd)**

XZ 5 µm / 15 µm / 45 µm

5 µm / 15 µm / 45 µm

(C)

Nerve Fiber Length (µm)

Epithelial layer

500 400 300 200 100 0

**

BL 42 days

Subbasal layer

500 400 300 200 100 0

**

BL 42 days

Stromal layer

500 400 300 200 100 0

BL 42 days

Figure 5. Corneal nerves abnormalities following corneal surface injury. (A, B) Full-thickness confocal images of mouse whole cornea stained with anti-β III tubulin antibody (*green*) at baseline (A) and 42 days after CSI-(B). *Red circle* denotes the area of corneal injury. *White boxes* represent corneal nerves in the central (I and III) and peripheral (II and IV) cornea. *Scale bar*: 250 µm. (Ia-IVd) Layers of corneal nerves are arranged by the following rows: (a) epithelial; (b) subbasal; (c) stromal; (d) 3D reconstruction. Neuromas (*arrowhead*) and beading (*arrow*) are shown. 3D reconstruction images of corneal nerves shown in XY, XZ, and YZ planes with color coded z-depth.

→

CSI Causes a Lasting Disruption of Corneal Innervation

We found that CSI first led to corneal nerve damage that peaked at 2 days, followed by a gradual recovery (regeneration) over the next 6 weeks. Also, CSI increased tortuosity, beading, and branching of corneal nerves. These changes resemble those observed in humans after corneal injury associated with transplant, refractive surgery, or corneal abrasion, and patients with ocular neuropathic pain exhibit similar phenotypes as assessed by in vivo confocal microscopy.[34,35] Moreover, treatment with autologous serum tears resulted in normalization of corneal nerve morphology and decreased photoallodynia.[36] It was interesting that in our model the subbasal layer density remained decreased despite the quantitative recovery to baseline of nerve density in the other layers. This is consistent with other models of ocular surface injury (dry eye, vitamin D deficiency, post-refractive surgery, diabetic keratopathy) and it is thought to be related to a disruption in Bowman's layer, which serves as a scaffold for the subbasal plexus.[37–39] Three-dimensional reconstitution of corneal confocal images revealed that some of the epithelial terminals arise directly from the stromal nerves bypassing the subbasal area. Although we showed that weeks after CSI the density of nerves return to preinjury levels in the epithelial and stromal layers, the distribution of these new nerves was abnormal with large areas that remained deinnervated, neuroma formation and increased in length and beading. The current study describes a novel approach to model the pathologic changes associated with ocular injury in humans. We concluded that CSI produces a clinically-relevant and lasting disruption of terminal architecture following reinnervation. This defines a quantitative and morphologic assay to study neuropathy in this corneal surface injury model.

CSI Induces Corneal Hypersensitivity

CSI increased sensitivity to local application of hypertonic saline. This is consistent with previous models of corneal injury-induced eye pain. For example, either ultraviolet (UV) irradiation or chronic application of benzalkonium chloride (BAC) produces pain-like behavior, including hypertonic saline-evoked eye-wiping.[40–42] In our model, the hyperalgesia resolved 14 days after CSI. This is substantially longer than previous reports describing enhanced eye-wiping behavior that lasted just 3 to 7 days following application of BAC and UV irradiation of the cornea.[40,41,42] This could be related to that fact that alkali-induced CSI damages nerves in all layers of the cornea, representing a much more extensive injury compared to the BAC and UV models, both of which affect the more superficial layers of the cornea.

Possible Mechanisms of the Initial CSI-Induced Corneal Hypersensitivity

Our CSI model caused hyperalgesia starting as early as 2 days after injury. This heightened nociceptive response occurred despite the absence of nerve terminals at the central cornea (Fig. 2C). This suggested that adjacent uninjured nociceptors in the peripheral cornea may contribute to secondary hyperalgesia, which is thought to be mediated by peripheral and central sensitization. Indeed, UV irradiation sensitizes corneal nociceptors, and chronic application of BAC and alkali burn to the ocular surface all have been shown to cause sensitization involving the TG and brainstem trigeminal nucleus.[32,40–42]

CSI Induces Chronic Ocular Neuropathic Pain

CSI produces an early hypersensitivity to hypertonic saline that resolves within 14 days and remains at baseline up to 6 weeks post-injury. This contrasts with a much longer-lasting pathology of corneal deinnervation and reinnervation. We proposed several explanations for this relationship: (1) anatomical changes are unrelated to ocular pain, (2) the aberrant regeneration of corneal nerves might mediate the resolution of pain behavior by an unidentified mechanism, and (3) a long-lasting sensitization of corneal nociceptive transmission develops that is masked by an upregulation of pain inhibitory mechanisms unrelated to corneal reinnervation abnormalities. The latter is supported by our observation that systemic administration of naltrexone 10 weeks after injury causes reinstatement of the corneal hypersensitivity and an associated increase in pERK activity in the TG neurons.
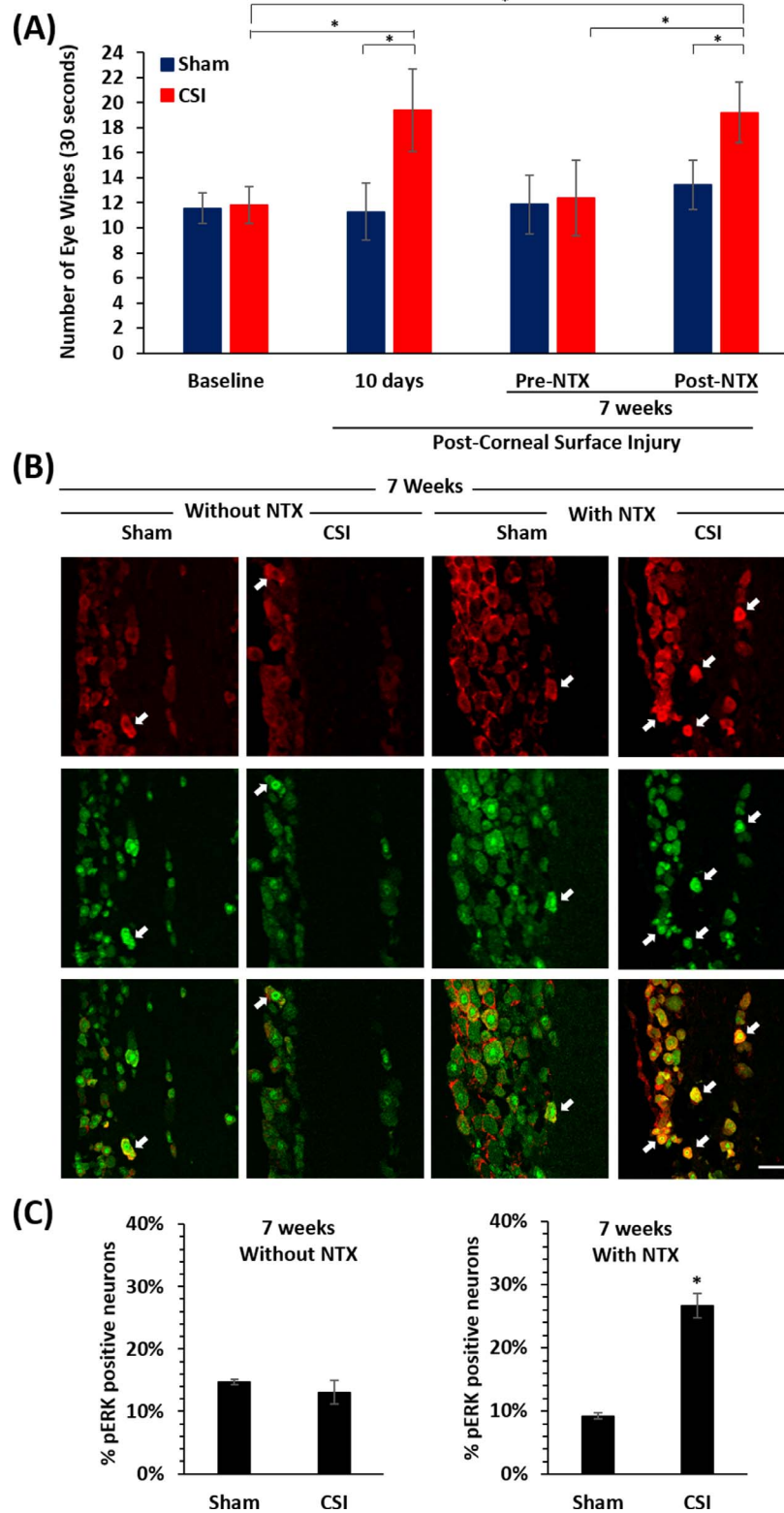
Figure 6. NTX unmasks corneal surface injury-induced neuronal sensitization. (A) 2M NaCl-induced eye-wiping behavior in sham ($n = 7$) and CSI (0.75N NaOH; $n = 5$) groups at baseline, 10 days, and 7 weeks after CSI before and after subcutaneous administration of NTX (3 mg/kg). Linear mixed models were used to compare the groups over time (*$P < 0.05$). (B) Representative images of ophthalmic division (V1) of the TG at 7 weeks after CSI without NTX (*left columns*) and with NTX (*right columns*; $n = 3$/group): (*Top*) pERK-positive cells in red,
→

←
(*Middle*) NeuN-positive cells in green, (*Bottom*) colocalization of pERK and NeuN cells in *yellow* (*arrow*). *Scale bar*: 50 μm. (C) Percentage of pERK-positive neurons (B; *yellow*) in sham and CSI groups ($n = 3$/group). Student's *t*-tests were used to compare %pERK-positive neurons between groups (*$P < 0.05$). The data are presented as mean±SEM.

Extracellular signal-regulated kinase (ERK), a mitogen-activated protein kinase (MAPK), is phosphorylated in neurons by noxious stimulation or tissue injury.[43] ERK phosphorylation is essential for the development of neuronal sensitization that contributes to hypersensitivity.[44] Multiple trigeminal nerve damage-associated chronic pain models have reported pERK-expressing neurons in the trigeminal system. For example, increased pERK expression was observed in V2 and V3 branches of the TG after injection of calcitonin gene-related peptide (CGRP) or CFA into the TMJ capsule as well as after partial infraorbital nerve ligation (pIONL).[45–48] In addition, a recent study showed that corneal alkali burn injury induced spontaneous ocular pain and increased pERK expression in the trigeminal nucleus at the central nervous system, including the subnucleus caudalis/upper cervical cord (Vc/V1), anterior cingulated cortex (ACC), insular cortex, and rostroventral medulla.[32] Together these data indicate that chronic ocular pain is masked by opioid receptor mediated latent sensitization.

Furthermore, our data showing that NLX-me, a peripheral opioid receptor antagonist, also reinstates ocular pain supported the hypothesis that recovery from ocular pain happens after the establishment of peripheral LS in this model. This raises the intriguing possibility that peripheral LS contributes to chronic ocular pain. We speculated that failure to develop or maintain compensatory opioid receptor activation could explain the varied susceptibility to ocular pain development after eye surgery or injury. As previously discussed, chronic ocular pain periodically cycles or "flares-up" from time to time. This silenced sensitization seen in murine models mimics the apparent fluctuations in pain after injury. LS, then, might explain the remitting nature of chronic ocular pain that ensues after eye trauma. Our finding that systemic and topical opioid antagonists reinstate ocular pain in injured mice, but not in sham-treated mice, unveils a new potential diagnostic and therapeutic opportunity to distinguish chronic ocular pain from dry eye and acute ocular pain. Beyond episodic pain, the failure of endogenous opioid receptor signaling could be a neuropathologic basis of persistent post-injury eye pain.
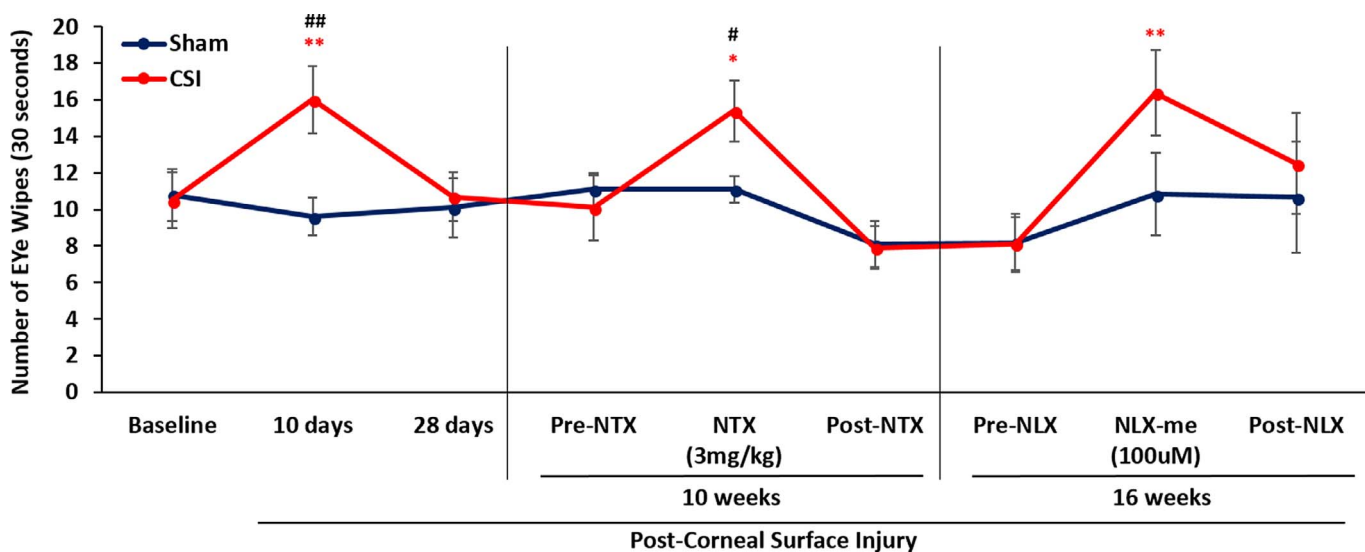
Figure 7. Corneal surface injury mediates peripheral latent sensitization that masks chronic ocular pain. Eye-wiping behavior of sham (*n* = 6) and CSI (*n* = 8) mice at baseline and 10 days, 28 days, and 10 and 16 weeks after CSI with 2 M NaCl stimulus. On week 10, NTX (3 mg/kg) was subcutaneously administered before eye-wiping test, and at 16 weeks NLX-me (100 μM) was topically applied to the ocular surface before ocular stimulation with hypertonic saline. Linear mixed models were used to compare the groups over time (between sham and CSI, #$P < 0.05$, ##$P < 0.01$, within CSI, *< 0.05, **$P < 0.01$). The data are presented as mean±SEM.

Summary and Conclusions

In summary, we present a model of ocular neuropathic pain that exhibits LS. Our data are consistent with a growing body of literature showing that chronic ocular pain is more complex than mere ocular surface dryness and suggests that long-lasting neurosensory changes are critical for the development of chronic ocular pain.[7,35,49–52] We concluded that our experimental model of chronic eye pain may be useful in elucidating underlying pathophysiology, developing novel diagnostic methods, and discovering new therapeutic targets for chronic eye pain.

Our work revealed a new diagnostic and therapeutic target to prevent the transition from nerve injury-induced acute pain to chronic pain and to alleviate enhanced sensitivity in the chronic pain state. Future studies should focus on determining methods to circumvent LS and to enhance the activity of mu-opioid receptors in the oculo-trigeminal system.

Acknowledgments

Disclosure: **J. Cho**, None; **N. Bell**, None; **G. Botzet**, None; **P. Vora**, None; **B.J. Fowler**, None; **R. Donahue**, None; **H. Bush**, None; **B.K. Taylor**, None; **R.J.C. Albuquerque**, None

References

1. Workshop DE. The epidemiology of dry eye disease: report of the Epidemiology Subcommittee of the International Dry Eye WorkShop (2007). *Ocul Surf*. 2007;5:93–107.
2. Galor A, Zlotcavitch L, Walter SD, et al. Dry eye symptom severity and persistence are associated with symptoms of neuropathic pain. *Br J Ophthalmol*. 2015;99:665–668.
3. Muller LJ, Marfurt CR, Kruse F, Tervo TM. Corneal nerves: structure, contents and function. *Exp Eye Res*. 2003;76:521–542.
4. Dieckmann G, Goyal S, Hamrah P. Neuropathic corneal pain: approaches for management. *Ophthalmology*. 2017;124:S34–S47.
5. Borsook D, Rosenthal P. Chronic (neuropathic) corneal pain and blepharospasm: five case reports. *Pain*. 2011;152:2427–2431.
6. Rosenthal P, Borsook D. The corneal pain system. Part I: the missing piece of the dry eye puzzle. *Ocul Surf*. 2012;10:2–14.
7. Rosenthal P, Borsook D. Ocular neuropathic pain. *Br J Ophthalmol*. 2016;100:128–134.
8. Wenk HN, Honda CN. Silver nitrate cauterization: characterization of a new model of corneal inflammation and hyperalgesia in rat. *Pain*. 2003;105:393–401.
9. Barabino S, Shen L, Chen L, Rashid S, Rolando M, Dana MR. The controlled-environment chamber: a new mouse model of dry eye. *Invest Ophthalmol Vis. Sci*. 2005;46:2766–2771.
10. Lin Z, Liu X, Zhou T, et al. A mouse dry eye model induced by topical administration of benzalkonium chloride. *Mol Vis*. 2011;17:257–264.
11. Stevenson W, Chen Y, Lee SM, et al. Extraorbital lacrimal gland excision: a reproducible model of severe aqueous tear-deficient dry eye disease. *Cornea*. 2014;33:1336–1341.
12. Bian F, Xiao Y, Zaheer M, Volpe EA, Pflugfelder SC, Li DQ, de Paiva CS. Inhibition of NLRP3 inflammasome pathway by butyrate improves corneal wound healing in corneal alkali burn. *Int J Mol Sci*. 2017:18(3).
13. Yan ZX, Luo Y, Liu NF. Blockade of angiopoietin-2/Tie2 signaling pathway specifically promotes inflammation-induced angiogenesis in mouse cornea. *Int J Ophthalmol*. 2017;10:1187–1194.
14. Galor A, Batawi H, Felix ER, Margolis TP, Sarantopoulos KD, Martin ER, Levitt RC. Incomplete response to artificial tears is associated with features of neuropathic ocular pain. *Br J Ophthalmol*. 2016;100:745–749.
15. Jacobs DS. Diagnosis and treatment of ocular pain: the ophthalmologist's perspective. *Curr Ophthalmol Rep*. 2017;5:271–275.
16. Solway B, Bose SC, Corder G, Donahue RR, Taylor BK. Tonic inhibition of chronic pain by neuropeptide Y. *Proc Natl Acad Sci U S A*. 2011;108:7224–7229.
17. Corder G, Doolen S, Donahue RR, et al. Constitutive mu-opioid receptor activity leads to long-term endogenous analgesia and dependence. *Science*. 2013;341:1394–1399.
18. Ormerod LD, Abelson MB, Kenyon KR. Standard models of corneal injury using alkali-immersed filter discs. *Invest Ophthalmol Vis. Sci*. 1989;30:2148–2153.

19. Klocek MS, Sassani JW, McLaughlin J, Zagon IS. Topically applied naltrexone restores corneal reepithelialization in diabetic rats. *J Ocul Pharmacol Ther*. 2007;23:89–102.

20. Albuquerque RJ, Hayashi T, Cho WG, et al. Alternatively spliced vascular endothelial growth factor receptor-2 is an essential endogenous inhibitor of lymphatic vessel growth. *Nat Med*. 2009;15:1023–1030.

21. Zudaire E, Gambardella L, Kurcz C, Vermeren S. A computational tool for quantitative analysis of vascular networks. *PLoS One*. 2011;6:e27385.

22. Launay PS, Godefroy D, Khabou H, et al. Combined 3DISCO clearing method, retrograde tracer and ultramicroscopy to map corneal neurons in a whole adult mouse trigeminal ganglion. *Exp Eye Res*. 2015;139:136–143.

23. Belmonte C, Gallar J, Pozo MA, Rebollo I. Excitation by irritant chemical substances of sensory afferent units in the cat's cornea. *J Physiol*. 1991;437:709–725.

24. Marvizon JC, Walwyn W, Minasyan A, Chen W, Taylor BK. Latent sensitization: a model for stress-sensitive chronic pain. *Curr Protoc Neurosci*. 2015;71:9.50.1–14.

25. Guan Y, Yuan F, Carteret AF, Raja SN, et al. A partial L5 spinal nerve ligation induces a limited prolongation of mechanical allodynia in rats: an efficient model for studying mechanisms of neuropathic pain. *Neurosci Lett*. 2010;471:43–47.

26. Bargagna-Mohan P, Paranthan RR, Hamza A. Withaferin A targets intermediate filaments glial fibrillary acidic protein and vimentin in a model of retinal gliosis. *J Biol Chem*. 2010;285:7657–7669.

27. Ferrari G, Bignami F, Giacomini C, et al. Ocular surface injury induces inflammation in the brain: in vivo and ex vivo evidence of a corneal-trigeminal axis. *Invest Ophthalmol Vis. Sci*. 2014;55:6289–6300.

28. Paschalis EI, Zhou C, Lei F, et al. Mechanisms of retinal damage after ocular alkali burns. *Am J Pathol*. 2017;187:1327–1342.

29. Paranthan R, Bargagna-Mohan P, Lau DL, Mohan R. A robust model for simultaneously inducing corneal neovascularization and retinal gliosis in the mouse eye. *Mol Vis*. 2011;17:1901–1908.

30. Wizeman JW, Nicholas AP, Ishigami A., Mohan R. Citrullination of glial intermediate filaments is an early response in retinal injury. *Mol Vis*. 2016; 22:1137–1155.

31. Wizeman JW, Mohan R. Expression of peptidyl-arginine deiminase 4 in an alkali injury model of retinal gliosis. *Biochem Biophys Res Commun* 2017;487:134–139.

32. Xiang Y, Zhou W, Wang P, et al. Alkali burn induced corneal spontaneous pain and activated neuropathic pain matrix in the central nervous system in mice. *Cornea*. 2017;36:1408–1414.

33. Farazifard R, Safarpour F, Sheibani V, Javan M. Eye-wiping test: a sensitive animal model for acute trigeminal pain studies. *Brain Res Brain Res Protoc*. 2005;16:44–49.

34. Patel DV, McGhee CN. In vivo confocal microscopy of human corneal nerves in health, in ocular and systemic disease, and following corneal surgery: a review. *Br J Ophthalmol*. 2009; 93:853–860.

35. Cruzat A, Qazi Y, Hamrah P. In vivo confocal microscopy of corneal nerves in health and disease. *Ocul Surf*. 2017;15:15–47.

36. Aggarwal S, Kheirkhah A, Cavalcanti BM et al. Autologous serum tears for treatment of photo-allodynia in patients with corneal neuropathy: efficacy and evaluation with in vivo confocal microscopy. *Ocul Surf*. 2015;13:250–262.

37. De Cilla S, Ranno S, Carini E, et al. Corneal subbasal nerves changes in patients with diabetic retinopathy: an in vivo confocal study. *Invest Ophthalmol Vis. Sci*. 2009;50:5155–5158.

38. Zhivov A, Winter K, Hovakimyan M, et al. Imaging and quantification of subbasal nerve plexus in healthy volunteers and diabetic patients with or without retinopathy. *PLoS One*. 2013;8: e52157.

39. Shetty R, Deshpande K, Deshmukh R, Jayadev C, Shroff R. Bowman break and subbasal nerve plexus changes in a patient with dry eye presenting with chronic ocular pain and vitamin D deficiency. *Cornea*.35:688–691.

40. Tashiro A, Okamoto K, Chang Z, Bereiter DA. Behavioral and neurophysiological correlates of nociception in an animal model of photokeratitis. *Neuroscience*. 2010;169:455–462.

41. Acosta MC, Luna C, Quirce S, Belmonte C, Gallar J. Corneal sensory nerve activity in an experimental model of UV keratitis. *Invest Ophthalmol Vis. Sci*. 2014;55:3403–3412.

42. Launay PS, Reboussin E, Liang H, et al. Ocular inflammation induces trigeminal pain, peripheral and central neuroinflammatory mechanisms. Neurobiol Dis 2016;88:16–28.

43. Ji RR, Baba H, Brenner GJ, Woolf CJ. Nociceptive-specific activation of ERK in spinal neurons contributes to pain hypersensitivity. *Nat Neurosci*. 1999;2:1114–1119.

44. Gao YJ, Ji RR. c-Fos and pERK, which is a better marker for neuronal activation and central sensitization after noxious stimulation and tissue injury? *Open Pain J*. 2009;2:11–17.

45. Cady RJ, Glenn JR, Smith KM, Durham PL. Calcitonin gene-related peptide promotes cellular changes in trigeminal neurons and glia implicated in peripheral and central sensitization. *Mol Pain*. 2011;7:94.

46. Csati A, Edvinsson L, Vecsei L, et al. Kynurenic acid modulates experimentally induced inflammation in the trigeminal ganglion. *J Headache Pain*. 2015;16:99.

47. Zhang Q, Cao DL, Zhang ZJ, Jiang BC, Gao YJ. Chemokine CXCL13 mediates orofacial neuropathic pain via CXCR5/ERK pathway in the trigeminal ganglion of mice. *J Neuroinflammation*. 2016;13:183.

48. Toyama M, Kudo C, Mukai C, et al. Trigeminal nervous system sensitization by infraorbital nerve injury enhances responses in a migraine model. Cephalalgia 2017;37:1317–1328.

49. Belmonte C, Acosta MC, Merayo-Lloves J, Gallar J. What causes eye pain? *Curr Ophthalmol Rep*. 2015;3:111–121.

50. Galor A, Levitt RC, Felix ER, Martin ER, Sarantopoulos CD. Neuropathic ocular pain: an important yet underevaluated feature of dry eye. *Eye (Lond)*. 2015;29:301–312.

51. Galor A, Covington D, Levitt AE, et al. Neuropathic ocular pain due to dry eye is associated with multiple comorbid chronic pain syndromes. *J Pain*. 2016;17:310–318.

52. Hamrah P, Qazi Y, Shahatit B, et al. Corneal nerve and epithelial cell alterations in corneal allodynia: an in vivo confocal microscopy case series. *Ocul Surf*. 2017;15:139–151.

translational vision science & technology